



# Development of the CMA-GFS-AERO 4D-Var assimilation system v1.0- Part 1: System description

Yongzhu Liu<sup>1,2,3</sup>, Xiaoye Zhang<sup>2,4</sup>, Wei Han<sup>1,2,3</sup>, Chao Wang<sup>1,2,3</sup>, Wenxing Jia<sup>2,4</sup>, Deying Wang<sup>2,4</sup>,  
Zhaorong Zhuang<sup>1,2,3</sup>, Xueshun Shen<sup>1,2,3</sup>

- 5 <sup>1</sup>CMA Earth System Modeling and Prediction Centre, China Meteorological Administration, Beijing, 10081, China  
<sup>2</sup>State Key Laboratory of Severe Weather, China Meteorological Administration, Beijing, 10081, China  
<sup>3</sup>Key Laboratory of Earth System Modeling and Prediction China Meteorological Administration, China Meteorological  
Administration, Beijing, 10081, China  
<sup>4</sup>Key Laboratory of Atmospheric Chemistry of CMA, Chinese Academy of Meteorological Sciences, Beijing, 10081, China  
10 *Correspondence to:* Xiaoye Zhang (xiaoye@cma.gov.cn), Xueshun Shen (shenxs@cma.gov.cn)

**Abstract.** We developed a strongly coupled chemistry meteorology four-dimensional variational (4D-Var) assimilation system, CMA-GFS-AERO 4D-Var, for investigating the feedbacks of chemical data assimilation on meteorological forecasts. This system was developed on the basis of the framework of the incremental analysis scheme of the China Meteorological Administration Global Forecasting System (CMA-GFS). CMA-GFS-AERO 4D-Var includes three component models:  
15 forward, tangent linear, and adjoint models. CMA-GFS-AERO forward model was constructed by integrating an aerosol module containing main physical processes of black carbon (BC) aerosol in the atmosphere into the CMA-GFS weather model. The tangent linear and the adjoint of the aerosol module was further developed and coupled online with the CMA-GFS tangent linear and adjoint models, respectively. In CMA-GFS-AERO 4D-Var, the BC mass concentration was used as the control variable and minimized together with atmospheric variables. The validation of this system includes the  
20 tangent linear approximation, the adjoint correctness test, the single-point observation ideal experiment and the full observation experiment. The results show that CMA-GFS-AERO tangent linear model performs well in tangent linear approximation for BC, and adjoint sensitivity agrees well with tangent linear sensitivity. Assimilating BC observations can generate analysis increments not only for BC but also for atmospheric variables, highlighting the capability of CMA-GFS-AERO 4D-Var in exploring the feedback effect of BC assimilation on atmospheric variables. The computational  
25 performance of CMA-GFS-AERO 4D-Var also indicates the potential in operational application. This study focuses on the theoretical architecture and practical implementation of the system, the detailed analysis of the batch test will be described in part 2 of this paper.

## 1 Introduction

Coupled chemistry meteorology models (CCMM) are atmospheric chemistry models that concurrently simulate  
30 meteorological processes and chemical transformations (Zhang, 2008; Baklanov et al., 2014; Bocquet, 2015). They are more recent compared to chemical transport models (CTM), which rely on meteorological fields as inputs (Seinfeld and Pandis,  
1



1998). Moisture and temperature perturbations to dynamics resulting from aerosol microphysics and radiative forcing are taken into consideration by CCMM, whereas CTMs lack the capability to incorporate these feedback mechanisms (Guerrette and Henze, 2015).

35 CCMM provides the possibility to assimilate both meteorological and chemical data, enabling to produce the optimal initial values for improving air quality predictions and developing re-analysis of three-dimensional (3D) chemical concentrations over the past decades (Bocquet, 2015). One of the first applications of data assimilation with a CCMM was conducted at Météo-France. Semane et al. (2009) used four-dimensional variational (4D-Var) data assimilation to assimilate the vertical profiles of ozone ( $O_3$ ) concentrations obtained from the AURA/MLS into the ARPEGE/MOCAGE chemistry meteorology  
 40 integrated system, and found that the assimilation of  $O_3$  reduces the wind bias in the lower stratosphere. This general approach is also adopted by the European Centre for Medium-range Weather Forecasts (ECMWF), although without considering the influence of chemical species on meteorological variables. Flemming et al. (2011) utilized the 4D-Var system of the Integrated Forecast System (IFS) coupled with three different  $O_3$  chemistry mechanisms, including a linear chemistry, the MOZART3 chemistry, and the TM5 chemistry, to assimilate  $O_3$  data from four satellite-borne sensors to improve the  
 45 simulation of the stratospheric  $O_3$  hole in 2008. Inness et al. (2013) used 4D-Var system of IFS coupled with the MOZART3 CTM to produce re-analysis of atmospheric concentrations of four chemical species, including CO,  $NO_x$ ,  $O_3$ , and formaldehyde (HCHO), over an 8-year period, and the data assimilation results showed notable improvements for CO and  $O_3$ , but little effect for  $NO_2$ , because of its shorter lifetime compared to those of CO and  $O_3$ . All the preceding studies have laid good foundations for data assimilation with CCMM. However, since CCMM are fairly recent, the development and  
 50 applications of data assimilation in CCMM are still limited. Further research and more attention are required, especially in terms of the potential feedbacks of chemical data assimilation on meteorological forecasts.

As a method widely used by international mainstream numerical prediction centers, 4D-Var is considered superior to three-dimensional variational (3D-Var) data assimilation, which ignores the time distribution of observations and assumes that observations within a time window are concentrated at the analysis moment (Lorenc and Rawlins, 2010). 4D-Var is an  
 55 extension of 3D-Var in the time dimension, it can consider the observation time more accurately and can implicitly propagate the initial background error covariance during the assimilation window (Lorenc and Rawlins, 2010). In the development of 4D-Var, the adjoint model (ADM) plays a crucial role by offering the sensitivity and gradient of the cost function with respect to the control variables. Elbern and Schmidt (1999) constructed the ADM of a 3D CTM (EUARD) for the first time. Inspired by this work, various ADM of CTM have been successively developed, mainly including CHIMERE (Menut et al.,  
 60 2000; Vautard et al., 2000; Schmidt and Martin, 2003), IMAGES (Müller and Stavrou, 2005), STEM-III (Sandu et al., 2005), CAMx (Liu, 2005), CMAQ (Hakami et al., 2007) and GEOS-Chem (Henze et al., 2007). An et al. (2016) and Wang et al. (2022) constructed the ADM of GRAPES-CUACE, an independently developed CCMM in China (Wang et al., 2010,



2018). ADM of these widely used CTM play an important role in inverse modelling and chemical data assimilation (Menut et al., 2000; Müller and Stavrou, 2005; Sandu et al., 2005; Hakami et al., 2007; Henze et al., 2009). However, these CTM  
65 do not take into account the influence between chemical species and meteorological variables, resulting in certain uncertainties in adjoint sensitivity, which in turn affects the effectiveness of 4D-Var. Although GRAPES-CUACE is a CCMM, its ADM only includes the adjoint of the chemical model and not the adjoint of the meteorological model, leading to uncertainties in the sensitivity calculation as well.

Black carbon (BC) aerosol is one of the major components of  $PM_{2.5}$ , mainly from incomplete combustion of biomass and  
70 fossil fuels (Kuhlbusch, 1998). As an important atmospheric pollutant, BC is porous and adsorbs other solid and gaseous pollutants (e.g.,  $SO_2$ ,  $O_3$ , etc.), and provides catalytic conditions for them, which plays an important role in photochemical and heterogeneous reactions and gas-particle conversion processes (Koch, 2001). BC is also the main optically absorbing component of atmospheric aerosols, effectively absorbing solar radiation in the visible to infrared wavelength range, thus affecting surface temperature. The climatic effects of BC have been widely reported, but the extent to which it affects  
75 weather forecasting requires further investigation (Chung and Seinfeld, 2002; Menon et al., 2002; Bond et al., 2013).

To deeply investigate the feedbacks of chemical data assimilation on meteorological forecasts, we utilized BC as a starting point to develop the strongly coupled chemistry meteorology 4D-Var system. Firstly, we constructed a CCMM system, named CMA-GFS-AERO, by integrating an aerosol module (AERO-BC) containing main aerosol physical processes of BC in the atmosphere into the operational version of the weather model CMA-GFS V4.0 (Shen et al., 2023), which was  
80 developed by the China Meteorological Administration (CMA). Then, the tangent linear and the adjoint of the AERO-BC module was constructed and coupled online with the tangent linear model (TLM) and ADM of CMA-GFS (Liu et al., 2017, 2023; Zhang et al., 2019), respectively. Thus, CMA-GFS-AERO ADM includes not only the adjoint of physical processes of BC, but also the adjoint of the meteorological model. Moreover, the BC adjoint variables and the meteorological adjoint variables mutually influence each other throughout the adjoint integration process, leading to a notable enhancement in the  
85 precision of adjoint sensitivity of chemistry and meteorology state. Based on the CMA-GFS-AERO CCMM and its TLM and ADM, we further constructed the CMA-GFS-AERO 4D-Var by adding the control variable of BC into the incremental analysis scheme of CMA-GFS 4D-Var. The rationality and capability of CMA-GFS-AERO 4D-Var in capturing the feedbacks of chemical data assimilation on meteorological analysis were verified using the single-point observation ideal experiment and the full observation experiment. The following part is divided into four sections. Section 2 introduces the  
90 methods, Section 3 describes the development of CMA-GFS-AERO 4D-Var, Section 4 presents the results, and the conclusions are found in Section 5.



## 2 Methodology

### 2.1 Model description

#### 2.1.1 CMA-GFS

95 The China Meteorological Administration Global Forecasting System (CMA-GFS, formerly known as GRAPES-GFS) is an operational global numerical weather model independently developed by the CMA (Chen and Shen, 2006; Chen et al., 2008; Shen et al., 2023). For this work, we used CMA-GFS version 4.0 (CMA-GFS v4.0). The dynamic core of CMA-GFS utilizes the fully compressible non-hydrostatical equations formulated on spherical coordinate with latitude and longitude, and adopts the height-based, terrain-following coordinate which is shown in Fig. S1 (Yang et al., 2007). The model employs  
 100 semi-implicit and semi-Lagrangian in two-level time integration (Yang et al., 2007). The spatial differential adopts Arakawa-C grid in the horizontal, and Charney-Philips variable staggering in the vertical. The large-scale transport processes utilize a hybrid Piecewise Rational Method (PRM) and Quasi-Monotone Semi-Lagrangian (QMSL) scheme (Su et al., 2013). The physical parameterization schemes are freely combinable, which principally include cumulus convection, microphysical precipitation, radiative transfer, land surface and boundary layer processes. The state variables of the CMA-GFS nonlinear  
 105 model (NLM) include non-dimensional pressure ( $\pi$ ), potential temperature ( $\theta$ ), the east-west component of horizontal wind ( $u$ ), the north-south component of horizontal wind ( $v$ ), the vertical component of wind ( $\hat{w}$ ), and the specific humidity ( $q$ ).

#### 2.1.2 CUACE

CUACE (CMA Unified Atmospheric Chemistry Environmental Forecasting System) is an air quality model developed by the Chinese Academy of Meteorological Sciences to study both air quality forecasting and climate change (Gong and Zhang,  
 110 2008; Wang et al., 2010; Zhou et al., 2012). CUACE mainly includes three modules: the aerosol module, the gaseous chemistry module and the thermodynamic equilibrium module. CUACE adopts CAM (Canadian Aerosol Module; (Gong et al., 2003)), which employs the size-segregated multicomponent aerosol algorithm, as its aerosol module. CAM involves six types of aerosols: BC, sulfate (SF), nitrate (NI), sea salt (SS), organic carbon (OC) and soil dust (SD), and each of them utilizes the sectional representation method to represent particle size distributions. The core of CAM is the major aerosol  
 115 processes in the atmosphere, including hygroscopic growth, coagulation, nucleation, condensation, dry deposition/sedimentation, and below-cloud scavenging.

### 2.2 Incremental 4D-Var

The CMA-GFS 4D-Var data assimilation system has been in operation at CMA since 1 July 2018 (Zhang et al., 2019). CMA-GFS 4D-Var applies the incremental analysis scheme proposed by Courtier et al. (1994). The cost function is defined  
 120 as





$$J(\delta x) = \frac{1}{2} \delta x^T \mathbf{B}^{-1} \delta x + \frac{1}{2} \sum_{i=0}^n (\mathbf{H}_i \mathbf{M}_{0 \rightarrow i} \delta x + d_i)^T \mathbf{R}_i^{-1} (\mathbf{H}_i \mathbf{M}_{0 \rightarrow i} \delta x + d_i) + J_c, \quad (1)$$

where  $\delta x = x_a - x_b$  represents the analysis increment of the model variables,  $x_a$  is the analysis field,  $x_b$  is the background state,  $d_i = \mathbf{H}_i \mathbf{M}_{0 \rightarrow i}(x_b) - y_i$  is the observation increment at time  $i$ ,  $y_i$  is the observation at time  $i$ ,  $\mathbf{H}_i$  represents the observation operator at time  $i$ ,  $\mathbf{M}_{0 \rightarrow i}$  denotes the model integration from the analysis time to time  $i$ ,  $\mathbf{H}_i$  is the linear operator corresponding to  $\mathbf{H}_i$ ,  $\mathbf{M}_{0 \rightarrow i}$  is the linear operator corresponding to  $\mathbf{M}_{0 \rightarrow i}$ ,  $\mathbf{B}$  represents the error covariance matrix of  $x_b$ ,  $\mathbf{R}_i$  denotes the observation error covariance matrix at time  $i$ , and  $J_c$  is the weak constraint term on the basis of the digital filter.  $J_c$  is not relevant to the current work, so the formula described below omits  $J_c$  term from the cost function for the sake of simplicity.

After the physical and preconditioning transformations of the control variables, the cost function can be expressed as

$$J(w) = \frac{1}{2} w^T w + \frac{1}{2} \sum_{i=0}^n (\mathbf{H}_i \mathbf{M}_{0 \rightarrow i} U w + d_i)^T \mathbf{R}_i^{-1} (\mathbf{H}_i \mathbf{M}_{0 \rightarrow i} U w + d_i), \quad (2)$$

where  $w$  denotes the control variables after the physical and preconditioning transformations, and the analysis increment is expressed as  $\delta x = U w$ ,  $U$  ( $U U^T = \mathbf{B}$ ) is the square root matrix of the background error covariance matrix after the physical and preconditioning transformations.

The gradient of the cost function  $J(w)$  with respect to the control variable  $w$  is

$$\nabla_w J = w + \sum_{i=0}^n U^T \mathbf{M}_{0 \rightarrow i}^T \mathbf{H}_i^T \mathbf{R}_i^{-1} (\mathbf{H}_i \mathbf{M}_{0 \rightarrow i} U w + d_i), \quad (3)$$

where  $\mathbf{H}_i^T$  is the adjoint operator of  $\mathbf{H}_i$ , and  $\mathbf{M}_{0 \rightarrow i}^T$  is the adjoint operator of  $\mathbf{M}_{0 \rightarrow i}$ , which denotes the inverse integration of the ADM from the time  $i$  to the analysis time.

Currently, the CMA-GFS 4D-Var system adopts a 6-h cycle and is performed four times a day, with assimilation windows of 0300 UTC-0900 UTC, 0900 UTC-1500 UTC, 1500 UTC-2100 UTC and 2100 UTC-0300 UTC. The assimilation process is divided into two parts: the outer loop and the inner loop. In the outer loop, the CMA-GFS NLM ( $\mathbf{M}_{0 \rightarrow i}$ ) is integrated at high resolution for 6 hours to obtain the trajectory, which is a collection of stored values of all model state variables at all time steps within the assimilation window. The observation increment  $d_i$  is calculated in the outer loop as well. In the inner loop, the CMA-GFS TLM and ADM are integrated at low resolution to calculate the cost function ( $J(w)$ ) and its gradient ( $\nabla_w J$ ).

The gradient is further provided to the Lanczos-CG algorithm (Lanczos, 1950; Liu et al., 2018) to perform the minimization, obtaining the optimal analysis increments to control variables.

### 3 Development of CMA-GFS-AERO 4D-Var

The computational cost is an important factor to be considered when developing a coupled chemistry meteorology 4D-Var system with potential for operational application (Flemming et al., 2015). The CUACE model is computationally expensive



150 since it includes more than one hundred chemical variables for aerosols and gases, as well as hundreds of gas-phase chemical reactions. It is difficult to construct a coupled chemistry meteorology 4D-Var system directly based on the CUACE model. On the other hand, BC has an important impact on the climate and can be used to study the two-way feedback interactions between chemistry and meteorology (Chung and Seinfeld, 2002; Menon et al., 2002; Bond et al., 2013). Therefore, we utilized BC as a starting point to construct the strongly coupled chemistry meteorology 4D-Var system (CMA-GFS-AERO

155 4D-Var).

Creating CMA-GFS-AERO 4D-Var required three important components: (1) CMA-GFS-AERO forward model, (2) CMA-GFS-AERO TLM and ADM, and (3) 4D-Var framework. This section provides a detailed description of the construction of the CMA-GFS-AERO 4D-Var from these three aspects.

### 3.1 CMA-GFS-AERO CCMM

160 In this work, for the sake of interest in BC and the consideration of computational efficiency, we extracted the codes related to BC from the CUACE model and converted them from Fortran 77 format to Fortran 90 format. Meanwhile, we also optimized the program structure and interface scalability, making it easier to be developed into tangent linear and adjoint codes. The resulting aerosol module is referred to as AERO-BC. The AERO-BC includes 18 subroutines in total: 1 emission flux program (*sf\_bc*), 4 vertical diffusion programs (*trac\_vert\_diff* and its subroutines), 6 programs related to the aerosol

165 physical processes of BC as mentioned in Section 2.1.2 (*aerosol\_bc* and its subroutines), and 7 programs related to the constant definitions and the parameter calculations. We further integrated the AERO-BC into CMA-GFS v4.0 by constructing interface programs (*black\_carbon* and *bc\_driver*). Thus, we obtained the CMA-GFS-AERO CCMM. The structure of the CMA-GFS-AERO model is shown in Fig. S2.

In the AERO-BC, BC is represented by 6 bins with particle diameters of 0.01-0.04, 0.04-0.16, 0.16-0.64, 0.64-2.56, 2.56-10.24, and 10.24-40.96  $\mu\text{m}$ , where the radius range is calculated by the geometric progression method to satisfy  $i = 1 + \ln[(r_i/r_1)^3]/\ln[V_{\text{RAT}}]$ , and  $V_{\text{RAT}}$  is the average volume ratio between adjacent bins (Jacobson et al., 1994). Thus, six new prognostic variables for the mass mixing ratio of BC, denoted as  $\psi_{bc}$  (unit: kg/kg), are added in the dynamical framework of CMA-GFS. The transport processes for  $\psi_{bc}$  are the same as that for the water-matter variables in CMA-GFS, using the hybrid PRM and QMSL schemes (Su et al., 2013). Besides, according to the vertical distribution characteristics of

175 BC in the MERRA-2 reanalysis data (<https://daac.gsfc.nasa.gov>) that the BC mass mixing ratio decreases rapidly in magnitude after entering the stratosphere to about  $10^{-12}$  kg/kg, which is 2-3 orders of magnitude smaller relative to the surface, we set the height of  $\psi_{bc}$  in the CMA-GFS-AERO model to 65 levels (about 30 hPa), approximately the middle layer of the stratosphere, to improve calculation efficiency and balance the memory usage and the effectiveness of BC forecast.



### 180 3.2 CMA-GFS-AERO TLM and ADM

In developing the TLM and ADM of the CMA-GFS-AERO model, we firstly constructed the tangent linear and adjoint codes of the AERO-BC module, subsequently coupled them with the TLM and ADM of CMA-GFS model (Liu et al., 2017, 2023; Zhang et al., 2019), respectively. The tangent linear and adjoint codes in this study were written line-by-line manually, without using any automatic differentiation tool.

185 The AERO-BC can be symbolically written as

$$Y = \mathbf{F}(C) \quad (4)$$

where  $\mathbf{F}$  denotes the AERO-BC model operator,  $C$  and  $Y$  are vectors representing the input and output variables of the AERO-BC, respectively.

190 The TL of the AERO-BC can be obtained by linearizing  $\mathbf{F}$ , expressed as

$$\delta Y = \mathbf{F} \delta C = \frac{\partial \mathbf{F}}{\partial C} \delta C, \quad (5)$$

where  $\mathbf{F}$  is the TL model operator,  $\delta C$  and  $\delta Y$  represent perturbations of input and output variables of the AERO-BC, respectively.

The AERO-BC TL contains the tangent linear programs corresponding to the emission flux, vertical diffusion, and aerosol physical processes as mentioned in Section 3.1. We further integrated the AERO-BC TL into the CMA-GFS TLM by constructing the interface program (tl\_black\_carbon and tl\_bc\_driver). The tangent linear of BC transport processes is the same as that for the water-matter variables in CMA-GFS TLM, using the tangent linear of QMSL. Thus, we obtained the CMA-GFS-AERO TLM.

The adjoint of the AERO-BC is essentially the transpose of the AERO-BC TL, expressed as

$$200 \quad \delta C^* = \mathbf{F}^T \delta Y^*, \quad (6)$$

where  $\mathbf{F}^T$  is the adjoint operator of  $\mathbf{F}$ ,  $\delta Y^*$  and  $\delta C^*$  represent input and output variables of the adjoint of AERO-BC, respectively.

The adjoint of AERO-BC, which includes the adjoint of the emission flux (ad\_sf\_bc), the adjoint of the vertical diffusion (ad\_trac\_vert\_diff and its subroutines), and the adjoint of aerosol physical processes of BC (ad\_aerosol\_bc and its subroutines), was coupled with the CMA-GFS ADM through the adjoint of the interface programs (ad\_black\_carbon and ad\_bc\_driver). The adjoint of BC transport processes is also the same as that for the water-matter variables in CMA-GFS ADM, using the adjoint of QMSL. In this way, we got the CMA-GFS-AERO ADM. The structure of CMA-GFS-AERO ADM is shown in Fig. S3.



### 3.3 CMA-GFS-AERO 4D-Var

On the basis of the CMA-GFS-AERO CCMM and its TLM and ADM, we further constructed the CMA-GFS-AERO 4D-Var by adding the control variable of BC into the incremental analysis scheme introduced in Section 2.2. We also provided a detailed introduction to the BC observation and errors, the BC observation operator, and the background error covariance for BC.

#### 3.3.1 BC mass concentration as control variable

The establishment of a strongly coupled chemistry meteorology 4D-Var system based on the CMA-GFS 4D-Var requires the addition of atmospheric chemistry analysis. Although the six variables for the mass mixing ratio of BC ( $\psi_{bc}$ ) have been used in the CMA-GFS-AERO forward model, they can constitute a heavy burden for the analysis if they are all included in the control vector. The reasons for this, as mentioned by Benedetti et al. (2009), mainly include: (1) background error statistics would have to be generated for all variables separately, (2) the control vector would be significantly larger in size, which would consequently increase the cost of the iterative minimization, and most importantly, (3) the BC analysis would be under constrained since the surface observations of BC are mass concentrations (unit:  $\mu\text{g}/\text{m}^3$ ), which do not distinguish between size bins, resulting in one observation of BC mass concentration being used to constrain six BC variables. To address these issues, the BC mass concentration is selected as the control variable, denoted as  $C_{bc}$  (unit:  $\mu\text{g}/\text{m}^3$ ), and is added to the control vector ( $x_u = (\psi, \chi_u, \pi_u, q)^T$ ,  $\psi$  is the stream function,  $\chi_u$  is the unbalanced velocity potential,  $\pi_u$  is the unbalanced Exner pressure, and  $q$  is the specific humidity) of CMA-GFS 4D-Var. Thus, the control vector for the CMA-GFS-AERO 4D-Var is  $x_u = (\psi, \chi_u, \pi_u, q, C_{bc})^T$ , assuming that these five variables are independent of each other.

The conversion relationship between  $C_{bc}$  and  $\psi_{bc}$  is

$$C_{bc} = \sum_{n=1}^6 \psi_{bc}^n * \rho * 10^9, \quad (7)$$

where  $\rho$  is the atmospheric density,  $n$  denotes the size bin of BC, and  $\psi_{bc}^n$  represents the BC mass mixing ratio for size bin  $n$ . In order to obtain the BC initial field that can be used in the CMA-GFS-AERO model from the analysis field, it is also necessary to convert  $C_{bc}$  to  $\psi_{bc}^n$ . Firstly, calculating the distribution weight ( $\omega^n$ ) of each size bin of  $\psi_{bc}^n$  in the background field following the equation  $\omega^n = \frac{\sum_1^N \psi_{bc}^n}{\sum_{n=1}^6 (\sum_1^N \psi_{bc}^n)}$ , where  $N$  represents the number of three-dimensional grid points. Secondly, calculating the analysis increment of  $\psi_{bc}^n$  ( $\delta\psi_{bc}^n$ ) based on the analysis increment of  $C_{bc}$  ( $\delta C_{bc}$ ), following the equation

$$\delta\psi_{bc}^n = \omega^n * \frac{\delta C_{bc}}{\rho * 10^9}, \quad (8)$$

Finally,  $\delta\psi_{bc}^n$  is interpolated and superimposed on  $\psi_{bc}^n$  in the background field to obtain the initial field of BC.

Similarly, in the minimization process of the inner loop of CMA-GFS-AERO 4D-Var, the conversion between the tangent linear variable of BC ( $\delta\psi_{bc}$ ) and the analysis increment of  $C_{bc}$  ( $\delta C_{bc}$ ) is also calculated according to the derivative of Eq. (7)



$$(\delta C_{bc} = \sum_{n=1}^6 \delta \psi_{bc}^n * \rho * 10^9) \text{ and Eq. (8).}$$

### 240 3.3.2 BC observation and errors

The BC observations used in the CMA-GFS-AERO 4D-Var system are the BC surface concentrations obtained from the China Atmospheric Monitoring Network (CAWNET), which was established by the CMA and has been monitoring the BC surface mass concentration in China since 2006 (Xu et al., 2020). The BC observation data were collected from 32 stations (Guo et al., 2020), and the distribution of these stations is shown in Fig. S4. The BC observation instrument of CAWNET is the AE31 BC meter produced by Magee, USA, which uses continuous optical grayscale measurement method to calculate BC concentration in real time (Gong et al., 2019). The BC concentrations adopted here are hourly averages. They have undergone strict quality control before use and several invalid sites have been eliminated.

The observation error covariance matrix  $\mathbf{R}$  in Eq. (1) contains both measurement and representativeness errors. Following the formula described by Chen et al. (2019), which is an improvement on the method proposed by Pagowski et al. (2010) and Schwartz et al. (2012), we calculated the measurement error  $\varepsilon_0$ . The formula is expressed as

$$\varepsilon_0 = 1.0 + 0.0075 \times O_{bc}, \quad (9)$$

where  $O_{bc}$  denotes the observed BC concentrations (unit:  $\mu\text{g}/\text{m}^3$ ).

Representativeness errors reflect the inaccuracies in the forward model and in the interpolation from the model grid to the observation location. We used the representativeness error ( $\varepsilon_r$ ) expression defined by Elbern et al. (2007) as follow

$$\varepsilon_r = \gamma \varepsilon_0 \sqrt{\frac{\Delta x}{L}}, \quad (10)$$

where  $\gamma$  is an adjustable parameter scaling  $\varepsilon_0$  ( $\gamma = 0.5$  was used here),  $\Delta x$  is the grid spacing (100 km in this work), and  $L$  is the radius of influence of a BC observation (set to 10 km here). The total BC observation error ( $\varepsilon_{bc}$ ) was defined as

$$\varepsilon_{bc} = \sqrt{\varepsilon_0^2 + \varepsilon_r^2}, \quad (11)$$

which constituted the diagonal elements in the  $\mathbf{R}$  matrix.

### 260 3.3.3 BC observation operator

The observation operator in the CMA-GFS-AERO 4D-Var system performs two basic tasks: (1) transforming model state variables into observed physical quantities, and (2) interpolating the background field (or analysis field) to the location of the observation. The transformation of the physical quantities is related to the type of observations, and the spatial interpolation operator consists of both horizontal and vertical interpolation. Since the CMA-GFS-AERO 4D-Var system adopts Charney-Philips variable staggering in the vertical direction and Arakawa-C grid in the horizontal direction, in the physical transformation of the observation operator, point jumps in the horizontal direction and layer jumps in the vertical direction should be performed according to the location of each element to reduce the errors introduced by variable transformation and spatial interpolation. The steps to construct the BC observation operator are as follows:



(1) Based on Eq. (7), the BC mass mixing ratios ( $\psi_{bc}$ ) of six size bins are accumulated and converted into the mass concentrations ( $C_{bc}$ ), which are further interpolated to the observation locations by the horizontal bilinear interpolation to obtain the equivalent BC concentrations that are consistent with the units of the observations.

(2) According to the heights of BC surface observations, the corresponding vertical interpolation schemes are selected to obtain the equivalent BC observations. If the height of BC surface observation is greater than the height of the first model layer, the cubic spline interpolation is used to process the BC concentration interpolation. If the observation height is less than the height of the first model layer, and the difference between the two heights is less than 300 meters, the BC concentration at the first model layer is regarded as the equivalent BC observation; while the difference between the two heights is greater than or equal to 300 meters, the data from that site is discarded.

### 3.3.4 Background error covariance for BC

The variable fields involved in variational assimilation are all three-dimensional, and it is challenging to directly deal with the correlations of these three-dimensional fields due to their high dimensionality. Therefore, in the CMA-GFS 4D-Var assimilation system, a simplification is made by assuming that the correlation coefficient can be expressed as the product of the vertical correlation coefficient and the horizontal correlation coefficient. And the horizontal correlation is calculated using the spectral filtering method, while the vertical correlation is calculated through EOF decomposition (Zhang et al., 2019).

In the CMA-GFS-AERO 4D-Var system, the background error covariance for the control variable BC adopts a modeled structure. The background error variance varies with height as shown in Fig. 1a. The vertical correlation model of the background error expressed as

$$R(z_i, z_j) = \frac{1}{1 + k_z(z_i - z_j)^2}, \quad (12)$$

where  $z_i$  and  $z_j$  are the model terrain heights of level  $i$  and  $j$ , respectively.  $k_z = \frac{g^2}{(RT_0)^2} k_p$ ,  $g$  denotes the gravitational acceleration,  $R$  represents the gas constant for dry atmospheric air,  $T_0$  is the standard temperature (273.15 K), and  $k_p$  is taken as 10 here for the control variable BC. Figure 1b depicts the distribution of the vertical correlation coefficients of the background error of the 1<sup>st</sup>, 10<sup>th</sup>, and 20<sup>th</sup> layers with other layers.

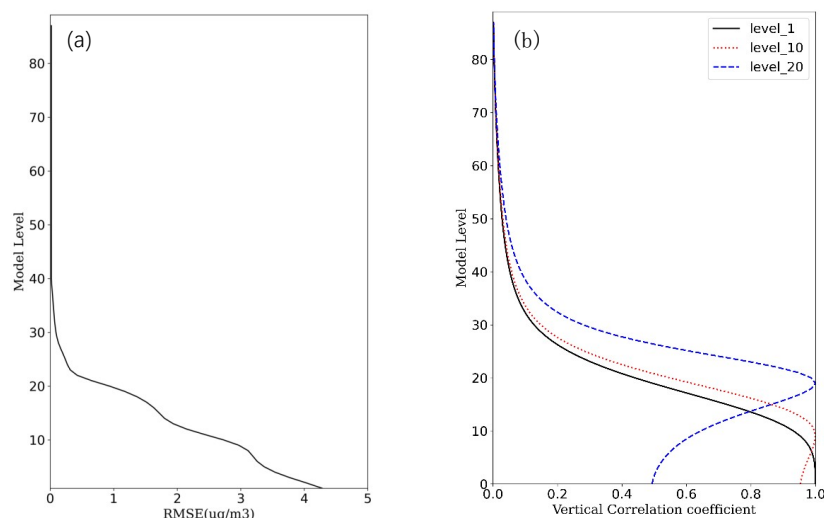


Figure 1: (a) Background error and (b) vertical correlation coefficients for BC.

The horizontal correlation of the background error for the control variable BC is calculated by the second-order auto-regressive (SOAR) correlation function, expressed as

$$r_{i,j} = \left(1 + \frac{d_{i,j}}{L}\right) \exp\left(-\frac{d_{i,j}}{L}\right), \quad (13)$$

where  $d_{i,j}$  is the arc length of the great circle between two points  $i$  and  $j$ ,  $L$  is the characteristic horizontal length scale, and the length scale for the control variable BC is referenced to the relationship between the length scale of humidity and the height in CMA-GFS 4D-Var, which is shown in Table 1.

Table 1: Characteristic horizontal length scales of the background error.

Height (km)	length scale (km)
0.50	165
1.43	172
5.56	175
10.5	209
16.3	234
23.9	234



## 4 Results

### 4.1 Model setup

In this work, the horizontal resolution of the CMA-GFS-AERO CCMM in the outer loop was set to  $0.25^\circ$ , with an integration step of 300 s, and the horizontal resolution of the CMA-GFS-AERO TLM and ADM in the inner loop was  $1.0^\circ$ , with an integration step of 900 s. The model has 87 vertical layers, with the top being approximately 0.1 hPa (Fig. S1). Referring to the running scheme of the CMA-GFS 4D-Var system described in Section 2.2, the CMA-GFS-AERO 4D-Var system also adopts a 6-h cycle and is performed four times a day, with assimilation windows of 0300 UTC–0900 UTC, 0900 UTC–1500 UTC, 1500 UTC–2100 UTC and 2100 UTC–0300 UTC. The forecast of the CMA-GFS-AERO model was restarted every 6 h from operational CMA-GFS analysis, with BC field initialized from null concentrations at 0300 UTC on October 1, 2016. The BC field at the end of a given 6 h forecast was passed as initial conditions to the next 6 h forecast. And the first 9 days were used as the spin-up time. The maximum minimization iteration number in the inner loop was set to 50. The atmospheric observations used in this work are shown in Table S1.

Anthropogenic emission sources used in this study were from the Multi-resolution Emission Inventory for China (MEIC) (Li et al., 2017; Zheng et al., 2018), the Copernicus Atmosphere Monitoring Service global and regional emissions (CAMS) (Granier et al., 2019), and the Task Force Hemispheric Transport of Air Pollution (HTAP) (Janssens-Maenhout et al., 2015) datasets at a global scale. These inventories include various gases ( $\text{NO}_x$ , CO,  $\text{SO}_2$ ,  $\text{NH}_3$ ,  $\text{CH}_4$  and NMVOC) and particulates (OC, BC,  $\text{PM}_{2.5}$  and  $\text{PM}_{10}$ ), which were processed into grid-point emission data applicable to the CUACE model through the EMIPS emission source processing system (Chen et al., 2023). To improve computational efficiency, they were further simplified into emission source data containing only BC as input to the CMA-GFS-AERO model. At present, we have run the CMA-GFS-AERO 4D-Var system for three months from October 1, 2016. This section mainly shows the experiment results of random time in these three months to present the rationality and stability of the system. The detailed results analysis of the batch test of the system will be further elaborated in part 2 of this paper.

### 4.2 Validation of CMA-GFS-AERO TLM and ADM

Validation of the tangent linear and adjoint models is an important part of introducing an adjoint model. Considering that CMA-GFS TLM and ADM have been validated and documented in Liu et al. (2017, 2023) and Zhang et al. (2019), here we mainly present the validation of tangent linear and adjoint of the newly developed AERO-BC module.

The correctness of the AERO-BC TL can be verified by checking whether the following equation is satisfied (Mahfouf and Rabier, 2000; Liu et al., 2017; Tian and Zou, 2020):

$$\Phi(\alpha) = \frac{\|F(C+\alpha\delta C) - F(C)\|}{\|F(\alpha\delta C)\|} = 1 + O(\alpha), \quad (14)$$

where  $\|\cdot\|$  denotes the norm of the vector,  $\alpha$  is the scale factor of initial perturbations with the range from 1.0 to  $10^{-14}$ . As





the scale factor  $\alpha$  becomes smaller and smaller, the function  $\Phi(\alpha)$  is expected to approach unity in an approximately linear way.

We firstly verified all submodules in the AERO-BC TL, finding that the tangent linear approximation of each submodule was correct. Subsequently, we conducted a set of six experiments with the integration time from 1 to 6 h to verify the correctness of the full AERO-BC TL. The background field and analysis increment generated by the CMA-GFS-AERO 4D-Var system were used as the basic-state initial field and the perturbation initial field of the CMA-GFS-AERO TLM for 6-hour forecasting. The atmospheric and BC state variables  $C$  and their perturbations  $\delta C$  of these six time periods were used as inputs of the AERO-BC and its TL, and the tangent linear approximation of the output variable (the perturbation of the mass mixing ratio of BC,  $\delta\psi_{bc}$ ) of the AERO-BC TL is tested using Eq. (14).

Figure 2 shows the results of the six correctness experiments. As expected, in each verification experiment, as the scale factor  $\alpha$  becomes smaller and smaller for certain ranges of  $\alpha$  values, the values of  $\Phi(\alpha)$  gradually get closer and closer to unity. When  $\alpha$  is too small (such as  $10^{-12}$ ), the accuracies of the  $\Phi(\alpha)$  values start to be affected by the machine round-off errors and drift away from unity. This indicates that the tangent linear approximation of the AERO-BC TL is correct.

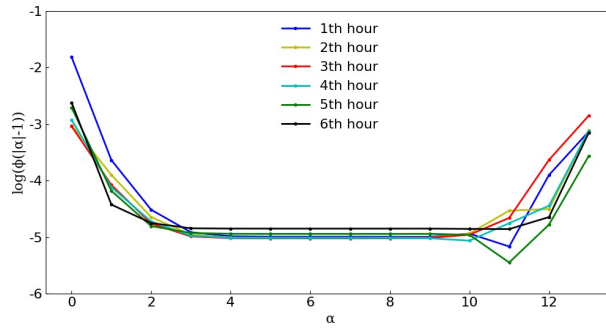


**Figure 2: Variations in the function  $|\Phi(\alpha) - 1|$  for the correctness check of the AERO-BC TL for the 6-h forecast length, where  $\alpha$  is the scale factor of initial perturbations.**

We further diagnosed the impact of linearized physical processes on the forecast effectiveness of CMA-GFS-AERO TLM.

Generally, the diagnostic method is to calculate the relative error ( $r$ ) between the tangent linear perturbation forecast  $\mathbf{M}(\delta x)$  and the nonlinear perturbation forecast  $\Delta\mathbf{M}(\delta x)$  (Mahfouf, 1999; Liu et al., 2019; Zhang et al., 2019), which can be expressed as

$$r = \frac{|\mathbf{M}(\delta x) - \Delta\mathbf{M}(\delta x)|}{\Delta\mathbf{M}(\delta x)}. \quad (15)$$

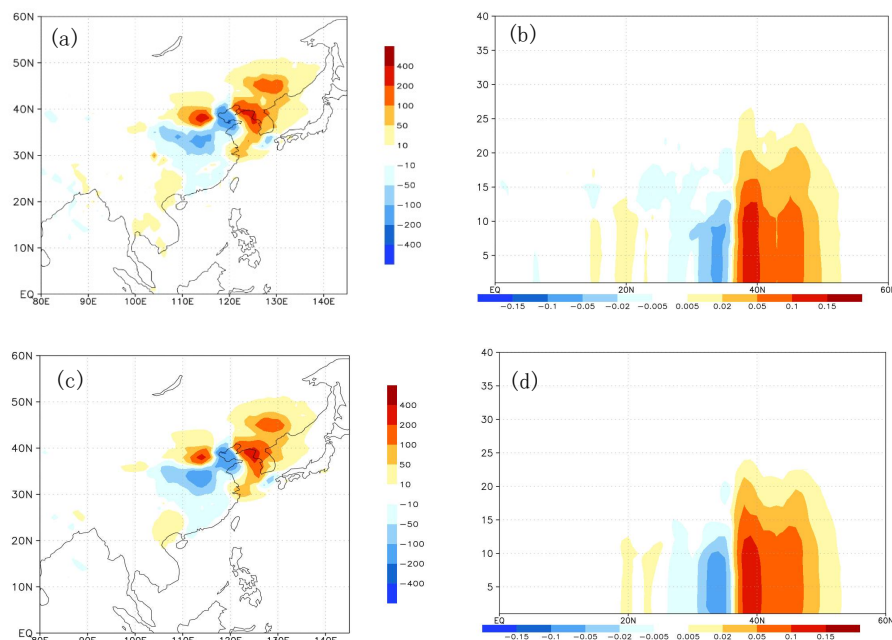
The nonlinear perturbation forecast  $\Delta\mathbf{M}(\delta x)$  is the difference between the NLM forecasts from two different initial conditions: the analysis filed  $x_a$  and the background filed  $x_b$ , that is  $\Delta\mathbf{M}(\delta x) = \mathbf{M}(x_a) - \mathbf{M}(x_b)$ . And the tangent linear



perturbation forecast  $\mathbf{M}(\delta x)$  is integrated using the analysis increment  $\delta x$  ( $\delta x = x_a - x_b$ ) as the initial perturbation field.  $r$  needs to be calculated for each model variable at each grid.

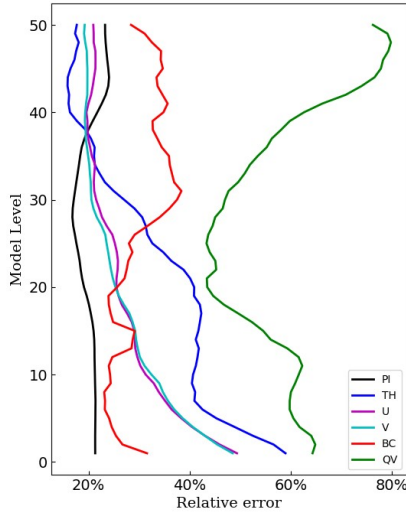
The forecast period for this experiment was 6 h starting from 0300 UTC on October 25, 2016 (randomly selected time). For the nonlinear perturbation test, which includes the full physical processes, the two initial conditions were the analysis field  $x_a$  and the background field  $x_b$  generated by the CMA-GFS-AERO 4D-Var system at 0300 UTC on October 25, 2016. For the tangent linear perturbation test, the initial condition was the analysis increment  $\delta x$  ( $\delta x = x_a - x_b$ ) at 0300 UTC on October 25, 2016. The model trajectory required for the tangent linear perturbation forecast was calculated by the CMA-GFS-AERO NLM including the full physical process with the background field  $x_b$  as the initial field. The nonlinear and tangent linear models were performed at the same resolution of  $1.0^\circ$ , and the analysis field  $x_a$  and the background field  $x_b$  were interpolated from  $0.25^\circ$  to  $1.0^\circ$  based on the 3D interpolation method (Huo et al., 2022).

Figure 3 depicts the results of the nonlinear perturbation forecast and the tangent linear perturbation forecast. Figure 3a-b show the differences in vertically accumulated and latitudinally averaged BC mass concentration (unit:  $\mu\text{g}/\text{m}^3$ ) after 6-h integration of the CMA-GFS-AERO NLM with two initial conditions of  $x_a$  and  $x_b$ , respectively, and Fig. 3c-d present the vertically accumulated and latitudinally averaged BC mass concentration perturbations after 6-h integration of CMA-GFS-AERO TLM with the initial condition of  $\delta x$  ( $\delta x = x_a - x_b$ ), respectively. It can be seen that after 6-h forecast, the distribution of the results of CMA-GFS-AERO NLM and TLM, both horizontally and vertically, are very similar with only minor differences. This indicates that CMA-GFS-AERO TLM shows good performance in tangent linear approximation for BC.



**Figure 3: Differences in (a) vertically accumulated and (b) latitudinally averaged BC mass concentration (unit:  $\mu\text{g}/\text{m}^3$ ) after 6-h integration of the CMA-GFS-AERO NLM with two initial conditions of  $x_a$  and  $x_b$ , and perturbations of (c) vertically accumulated and (d) latitudinally averaged BC mass concentration after 6-h integration of CMA-GFS-AERO TLM with the initial condition of  $\delta x$  ( $\delta x = x_a - x_b$ ).**

The vertical distribution of the globally averaged relative error between the perturbation forecasts of CMA-GFS-AERO TLM and NLM, which was calculated according to Eq. (15), is shown in Fig. 4. It can be seen that below the 20<sup>th</sup> model layer, the tangent linear approximation for BC is better than that for wind field, potential temperature, and specific humidity. Although the tangent linear approximation for BC is slightly worse above the 20<sup>th</sup> model layer, it is still far better than that for specific humidity. It's worth noting that the BC concentration above the 20<sup>th</sup> model level is quite low (Fig. 3b), so the impact of the tangent linear approximation is minimal. This phenomenon indicates that as a coupled variable similar to a physical process variable in the CMA-GFS-AERO model, the tangent linear approximation for BC is quite effective.



395 **Figure 4: The relative error in the CMA-GFS-AERO TLM with simple physics with respect to the NLM with full physics at the resolution of 1.0°. (black line: non-dimensional pressure, blue line: potential temperature, red line: BC, magenta line: u-wind, cyan line: v-wind; green line: specific humidity).**

The correctness of the AERO-BC adjoint can be verified by checking whether the following equation is satisfied (Mahfouf  
 400 and Rabier, 2000; Liu et al., 2017; Tian and Zou, 2020)

$$\langle \mathbf{F}(\delta C), \mathbf{F}(\delta C) \rangle = \langle \delta C, \mathbf{F}^T(\mathbf{F}(\delta C)) \rangle, \quad (16)$$

where  $\langle \cdot, \cdot \rangle$  denotes the inner product. Using  $\delta C$  as the input of the AERO-BC TL, the output of the AERO-BC TL  $\mathbf{F}(\delta C)$   
 can be obtained and the left-hand side (LHS) of Eq. (16) can be calculated. Then, taking  $\mathbf{F}(\delta C)$  as the input of the  
 AERO-BC adjoint, we can get its output  $\mathbf{F}^T(\mathbf{F}(\delta C))$  and calculate the right-hand side (RHS). If the AERO-BC adjoint is  
 405 developed correctly, the LHS and RHS of Eq. (16) is expected to agree with the machine accuracy of the data type declared  
 in the program, which is double precision in the AERO-BC.

Following Eq. (16), we set five experiments with the integration time equal to 1, 6, 12, 24, and 36 steps. Considering the  
 mass mixing ratio of BC ( $\psi_{bc}$ ) as an example, for each experiment, the atmospheric variables and  $\psi_{bc}$  perturbations in the  
 analysis increment generated by the CMA-GFS-AERO 4D-Var system was used as the input of the AERO-BC TL. We run  
 410 the tangent linear codes once to obtain the value of the tangent linear output, and calculated the LHS of Eq. (16). Then, taken  
 the tangent linear output as input, the AERO-BC adjoint codes was run once to obtain the sensitivity value, which further  
 was used to calculated the RHS of Eq. (16) with the  $\psi_{bc}$  perturbation. The validation results are presented in Table 2. The  
 resulting LHS and RHS from the five tests agree with the precision of machine accuracies, indicating the correctness of the



AERO-BC adjoint model.

415

**Table 2: Correctness check results of the newly developed AERO-BC adjoint model when it is integrated for 1, 6, 12, 24, and 36 steps.**

Step	LHS	RHS	(LHS-RHS)/LHS
1	6. 048801009887637E-015	6. 048801009887634E-015	5.2166431260112900E-16
6	5. 661147803064362E-015	5. 661147803064381E-015	3.3443150371477720E-15
12	5. 608184349558140E-015	5. 608184349558160E-015	3.6572234893387934E-15
24	5. 694921201673081E-015	5. 694921201673082E-015	1.3852007381406021E-16
36	5. 845344664075793E-015	5. 845344664075791E-015	2.6991082666833257E-16

LHS: left-hand side of Eq. (16); RHS: right-hand side of Eq. (16).

#### 420 4.3 Single-point observation ideal experiment

In order to evaluate the rationality of the CMA-GFS-AERO 4D-Var system, we set the single-point observation ideal experiment for BC. The experiment period was 6 h starting from 0300 UTC on November 24, 2016 (randomly selected time), and the forecast field of the CMA-GFS-AERO model at this time was selected as the background filed. During the assimilation process, no atmospheric observations were added. We adopted the BC surface observation at Nanjiao station (116.47°E, 39.8°N), which is located in Beijing, at 0300 UTC on November 24, 2016. The altitude of Nanjiao station is 31.3 meters, and the observed BC concentration is 10.0  $\mu\text{g}/\text{m}^3$ . Figure S5 shows the location of the BC observation and the wind field at 925hPa, which moves from northwest to southeast. The BC observation was set at 0300, 0600, and 0900 UTC, respectively, corresponding to the initial, the middle, and the end of the assimilation time window.

Theoretically, the analysis increment at the initial time for 4D-Var assimilation is  $\delta\mathbf{x} = \mathbf{B} \sum_{i=0}^n \mathbf{M}_{0 \rightarrow i}^T \mathbf{H}_i^T (\mathbf{H}_i \mathbf{M}_{0 \rightarrow i} \mathbf{B} \mathbf{M}_{0 \rightarrow i}^T \mathbf{H}_i^T + \mathbf{R}_i)^{-1} (-d_i)$ . If we only assimilate the observation at time  $t_i$ , the analysis increment at the observation time is  $\mathbf{M}_{0 \rightarrow i} \delta\mathbf{x} = \mathbf{M}_{0 \rightarrow i} \mathbf{B} \mathbf{M}_{0 \rightarrow i}^T \mathbf{H}_i^T (\mathbf{H}_i \mathbf{M}_{0 \rightarrow i} \mathbf{B} \mathbf{M}_{0 \rightarrow i}^T \mathbf{H}_i^T + \mathbf{R}_i)^{-1} (-d_i)$ . When assimilating the single point observation,  $(\mathbf{H}_i \mathbf{M}_{0 \rightarrow i} \mathbf{B} \mathbf{M}_{0 \rightarrow i}^T \mathbf{H}_i^T + \mathbf{R}_i)^{-1} (-d_i)$  is a vector with only one factor. If the observation position and the analysis grid coincide, the spatial interpolation in the observation operator can be ignored. Thus, the analysis increment at the observation time can reflect the structure of the background field error covariance  $\mathbf{M}_{0 \rightarrow i} \mathbf{B} \mathbf{M}_{0 \rightarrow i}^T$  at the observation time. Figure 5 shows the analysis increments of BC at the first model layer at the observation times, with the BC observation set at 0300, 0600, and 0900 UTC, respectively. When the BC observation is set at 0300 UTC (the observation increment  $(d_i = \mathbf{H}_i \mathbf{M}_{0 \rightarrow i}(\mathbf{x}_b) - y_i)$  is  $-1.2 \mu\text{g}/\text{m}^3$  at 0300 UTC), the 4D-Var assimilation is equivalent to the 3D-Var assimilation, and the horizontal distribution of the BC analysis increment is determined by the static background field error covariance model  $\mathbf{B}$ . Since the CMA-GFS-AERO



4D-Var system uses a homogeneous second-order autoregressive spatial correlation model, the BC analysis increment at 0300 UTC (Fig. 5a) is essentially isotropic, and only the background field error covariance, which varies with latitude, causes the analysis increments to differ somewhat in the north-south direction. When the BC observation is set at 0600 UTC (the observation increment is  $-9.5 \mu\text{g}/\text{m}^3$  at 0600 UTC) and 0900 UTC (the observation increment is  $-9.0 \mu\text{g}/\text{m}^3$  at 0900 UTC), the BC analysis increments show anisotropic characteristics (Fig. 5b-c), which is consistent with the movement of the wind at 925hPa (Fig. S5), indicating that the background field error covariance varies with the weather situation. Meanwhile, it can also be seen that the values of the BC analysis increments at 0600 and 0900 UTC are much larger than those at 0300 UTC. This is because the BC observation increments at 0600 and 0900 UTC are greater than those at 0300 UTC.

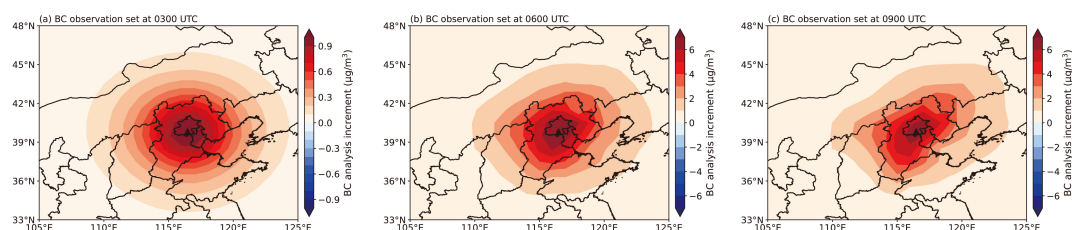


**Figure 5:** The analysis increments of BC at the first model level at the observation times, with the BC observation set at (a) the initial of the assimilation time window, 0300 UTC; (b) the middle of the assimilation window, 0600 UTC; (c) the end of the assimilation time window, 0900 UTC. The black triangle represents the ideal observation location (116.47°E, 39.8°N).

Figure 6 presents the evolved analysis increments of BC at the first model level at the end of the assimilation time window (0900 UTC) obtained by CMA-GFS-AERO TLM, with the BC observation set at 0300 and 0600 UTC, respectively. The BC analysis increments show a more similar horizontal distribution structure relative to the analysis increments at the observation time of 0900 UTC (Fig. 5c). This is because no matter what time the observation is set at, the spatial propagation of the observation information is achieved through the model integration.

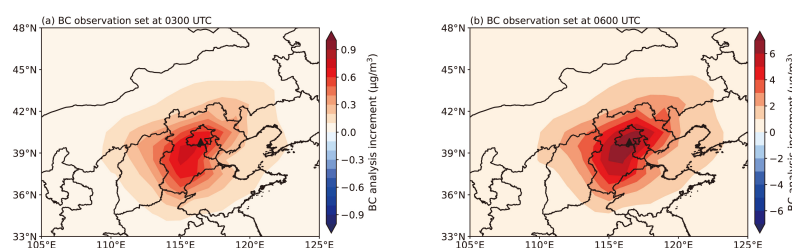


**Figure 6:** The analysis increments of BC at the end of the assimilation time window, 0900 UTC, with the BC observation set at (a) the initial of the assimilation window, 0300 UTC; (b) the middle of the assimilation window, 0600 UTC. The black triangle represents the ideal observation location (116.47°E, 39.8°N).



As mentioned above, when the BC observation is set at 0300 UTC, the 4D-Var assimilation is equivalent to the 3D-Var  
 465 assimilation. Since the BC variable is assumed to be uncorrelated with the atmospheric variables in the static  $\mathbf{B}$ , and there is  
 no direct relationship between the BC observation operator and the atmospheric variables, the BC observation does not lead  
 to the generation of the analysis increments of atmospheric variables. In this case, although the BC control variable is  
 minimized together with the atmospheric variables in the CMA-GFS-AERO 4D-Var system, it still cannot be considered as  
 the coupled assimilation in essence. Figure 7 depicts the analysis increments of temperature at the first model level at the  
 470 initial of the assimilation time window (0300 UTC), with the BC observation set at 0600 and 0900 UTC, respectively. It can  
 be seen that when the BC observation is set at 0600 and 0900 UTC,  $\mathbf{B}$  evolves within the assimilation time window through  
 the TLM  $\mathbf{M}_{0 \rightarrow i}$ , obtaining the implicit background error covariance matrix  $\mathbf{M}_{0 \rightarrow i} \mathbf{B} \mathbf{M}_{0 \rightarrow i}^T$  that evolves with time.  
 $\mathbf{M}_{0 \rightarrow i} \mathbf{B} \mathbf{M}_{0 \rightarrow i}^T$  includes the error co-correlation information of BC and atmospheric variables, and can realize the feedback of  
 the BC observation to the atmospheric variables through the CMA-GFS-AERO ADM  $\mathbf{M}_{0 \rightarrow i}^T$ , further producing positive  
 475 analysis increments of temperature, with the value of about 0.02 K near the observation location (Fig. 7). This indicates that  
 the temperature of the analysis field will increase due to the assimilation of the BC observation.

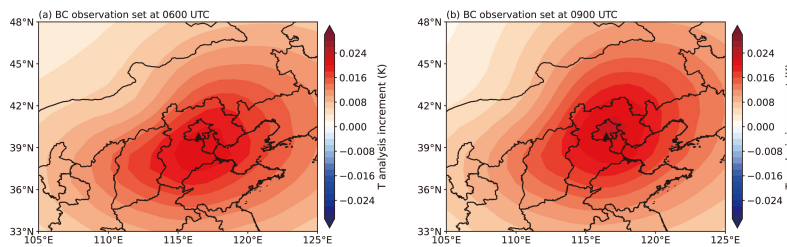


**Figure 7: The analysis increments of temperature at the first model layer at the initial of the assimilation time window, 0300 UTC, with the BC observation set at (a) the middle of the assimilation window, 0600 UTC; (b) the end of the assimilation time window, 0900 UTC. The black triangle represents the ideal observation location (116.47°E, 39.8°N).**

Figure 8 shows the analysis increments of pressure, east-west component of horizontal wind, and relative humidity at the first model level at the initial of the assimilation time window (0300 UTC), with the BC observation set at 0900 UTC. It is  
 485 obvious that the single-point BC observation assimilation produces a certain degree of analysis increments of pressure,  
 east-west component of horizontal wind, and relative humidity in North China, which shows that the CMA-GFS-AERO  
 4D-Var coupled assimilation system can reflect the impact of BC assimilation on atmospheric increments. In fact, the BC  
 observation is distributed within the assimilation time window, rather than just at a fixed moment, thus, the advantages of the  
 CMA-GFS-AERO 4D-Var strong coupling assimilation system can be fully utilized to explore the feedback effect of BC  
 490 assimilation on atmospheric variables.

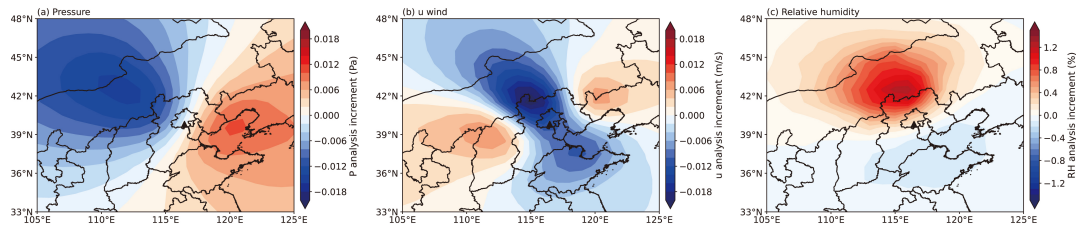


**Figure 8:** The analysis increments of (a) pressure, (b) east-west component of horizontal wind, and (c) relative humidity at the first model layer at the initial of the assimilation time window, 0300 UTC, with the BC observation set at the end of the assimilation time window, 0900 UTC. The black triangle represents the ideal observation location (116.47°E, 39.8°N).

#### 4.4 Case study on BC and atmosphere assimilation

On the basis of the single-point observation ideal experiment, we further set the full observation experiment for BC and atmospheric variables. The experiment period was also 6 h starting from 0300 UTC on November 24, 2016 (the same time as the experimental setup in Section 4.3), and the forecast field of the CMA-GFS-AERO model at this time was selected as the background filed. We conducted a set of four experiments, and the observations assimilated in each experiment are shown in Table 3. It's worth noting that in EXP3, operational meteorological observations were assimilated first, followed by BC surface observations, and atmospheric variables and the BC variable were minimized separately. This is actually the weakly coupled assimilation. While in EXP4, BC surface observations and operational meteorological observations were assimilated simultaneously, and the BC variable and atmospheric variables were minimized together, which is the strongly coupled assimilation. Different from the single-point observation ideal experiment in Section 4.3, in which the observations are placed at a fixed time, we assimilated all observations within the assimilation time window in the full observation experiment.

**Table 3: Design of four assimilation experiments.**

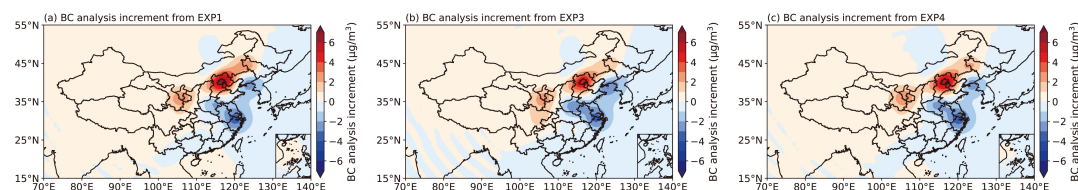
Experiments	Assimilated observations
EXP1	Only BC surface obs.
EXP2	Only operational meteorological obs.
EXP3	Operational meteorological obs. and BC surface obs., minimized separately
EXP4	Operational meteorological obs. and BC surface obs., minimized together

Figure 9 presents the analysis increments of BC at the first model layer from EXP1, EXP3, and EXP4. When only BC





surface observations are assimilated (EXP1), the BC analysis increment is mainly distributed in North China and Eastern China, with a maximum value of about  $6.0 \mu\text{g}/\text{m}^3$  (Fig. 9a). When both operational meteorological observations and BC surface observations are assimilated (EXP3 and EXP4), regardless of whether the BC variable and atmospheric variables are minimized together, the distribution and the value of BC analysis increments are basically consistent with EXP1, with slight differences (Fig. 9b-c). This implies the slight impact of assimilation of meteorological observations on BC analysis increments, and also indicates the similar assimilation effects of the weakly coupled assimilation and the strongly coupled assimilation on BC.



**Figure 9: The analysis increments of BC at the first model layer from (a) EXP1, (b) EXP3, and (c) EXP4.**

We further explored the impact of assimilating BC surface observations on analysis increments of atmospheric variables. Figure 10a, 10d, 10g, and 10j present the analysis increments of temperature, pressure, east-west component of horizontal wind, and relative humidity, respectively, at the first model layer from EXP1, showing the impact of assimilating only BC surface observations on the analysis increments of atmospheric variables. Figure 10b, 10e, 10h, and 10k are the analysis increments of these four atmospheric variables at the first model layer from EXP3, presenting the impact of assimilating BC surface observations on the analysis increments of atmospheric variables in the weakly coupled assimilation. Figure 10c, 10f, 10i, and 10l depict the differences of analysis increments of these four atmospheric variables between EXP4 and EXP2 (EXP4 minus EXP2), reflecting the impact of assimilating BC surface observations on the analysis increments of atmospheric variables in the strongly coupled assimilation. It can be seen that when only BC surface observations are assimilated (EXP1), there are certain degrees of analysis increments of temperature (Fig. 10a), pressure (Fig. 10d), east-west component of horizontal wind (Fig. 10g), and relative humidity (Fig. 10j) distributed in North China and Eastern China, which is consistent with the distribution of BC analysis increments (Fig. 9). The value of the analysis increments of temperature, pressure, east-west component of horizontal wind, and relative humidity can reach about  $0.1\text{K}$  (Fig. 10a),  $\pm 0.04\text{Pa}$  (Fig. 10d),  $-0.14\text{m/s}$  (Fig. 10g), and  $3.5\%$  (Fig. 10j), respectively. When both operational meteorological observations and BC surface observations are assimilated in a weakly coupled manner (EXP3), the distributions and the values of the analysis increments of these four atmospheric variables (Fig. 10b, e, h, k) are basically consistent with those of EXP1. This indicates that the impact of the weakly coupled assimilation on the analysis increments of atmospheric variables is almost the



same as the impact of assimilating only BC observations.

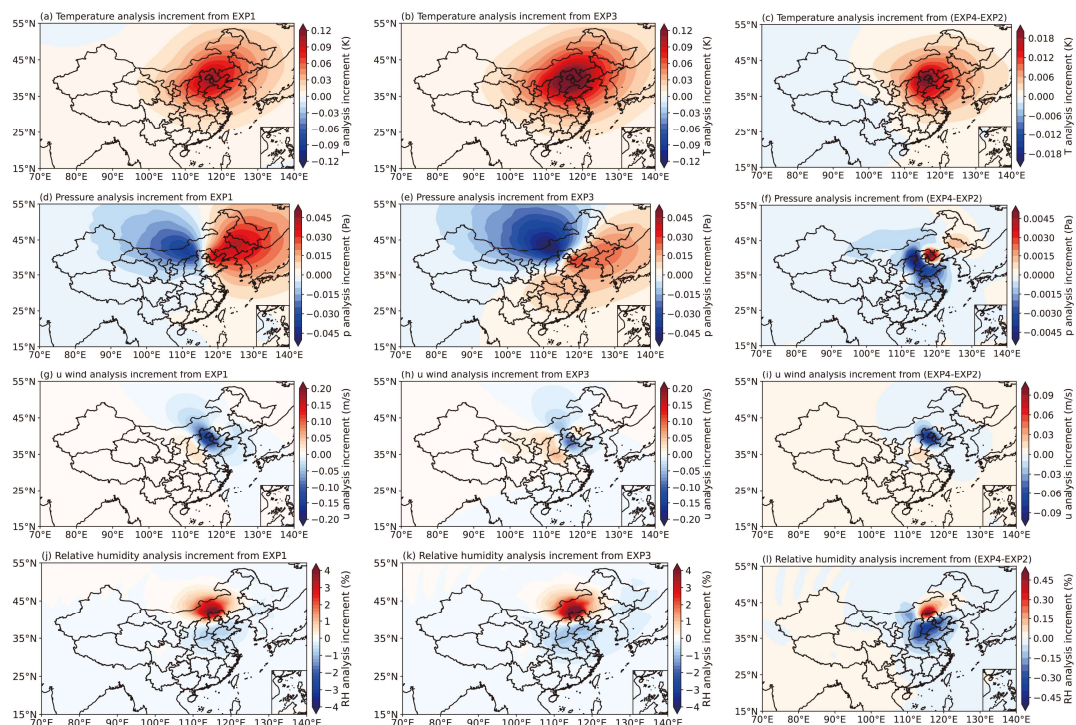


**Figure 10: The analysis increments of (a, b, c) temperature, (d, e, f) pressure, (g, h, i) east-west component of horizontal wind, and (j, k, l) relative humidity at the first model layer. (a, d, g, j) are analysis increments from EXP1, (b, e, h, k) are analysis increments from EXP3, and (c, f, i, l) are the differences in analysis increments between EXP4 and EXP2 (EXP4 minus EXP2).**

From the differences between EXP4 and EXP2, it can be found that the distribution of the analysis increments of temperature (Fig. 10c), pressure (Fig. 10f), east-west component of horizontal wind (Fig. 10i), and relative humidity (Fig. 10l) are similar to those of EXP1 and EXP3. Although the distribution of the pressure analysis increments is not as extensive as those of EXP1 and EXP3, it also shows a pattern of negative values in the west of North China and positive values in the east of North China. It is worth noting that the values in each sub-image of the right panel in Fig. 10 are about an order of magnitude smaller than those on the left and the middle. This implies that when both operational meteorological observations and BC surface observations are assimilated in a strongly coupled manner (EXP4), the feedback on atmospheric analysis is constrained by the atmospheric observations, resulting in the analysis increments being much smaller than assimilating BC observations alone and the weakly coupled assimilation. Therefore, when considering the feedback effect of BC assimilation on atmospheric analysis, it is necessary to assimilate atmospheric observations and BC observations in a strongly coupled manner, otherwise the feedback effect may be amplified.



4.5 Computational performance of CMA-GFS-AERO 4D-Var

560 This section presents the computational performance of CMA-GFS-AERO 4D-Var from three aspects: (1) forward model, (2) TLM and ADM, and (3) 4D-Var system. We firstly evaluated the computational performance of a CMA-GFS-AERO simulation and compared it with that of the CMA-GFS simulation. Table 4 shows the computational costs for 6 h, 24 h, and 120 h integrations of CMA-GFS and CMA-GFS-AERO models. It can be seen that for 6 h, 24 h, and 120 h forecasts with the same integration time step (300 s), the same horizontal resolution of 0.25°, and the same number of CPU cores (1920 cores), the CMA-GFS-AERO simulations increase only about 10% of the computational time of the CMA-GFS simulations. This shows the high efficiency of CMA-GFS-AERO CCMM, which is an important factor in developing a strongly coupled chemistry meteorology 4D-Var system.

Table 4: Computational costs (unit: s) for 6 h, 24 h, and 120 h integrations of CMA-GFS and CMA-GFS-AERO models.

Model/Integration time	6 h	24 h	120 h
CMA-GFS	111.5	366.6	1725.2
CMA-GFS-AERO	121.9	403.5	1930.5

570 Note: The CMA-GFS and CMA-GFS-AERO models are integrated with the same time step (300 s), the same horizontal resolution of 0.25°, and the same CPU cores (1920 cores).

Table 5 presents the computational costs for 12 h integrations of CMA-GFS TLM/ADM and CMA-GFS-AERO TLM/ADM, and Table 6 shows the computational costs for 6 h integrations of CMA-GFS 4D-Var and CMA-GFS-AERO 4D-Var. It is apparent that with an increasing number of CPU cores, the acceleration effects of CMA-GFS-AERO TLM, ADM, and 4D-Var are comparable to those of CMA-GFS TLM, ADM, and 4D-Var. When using 1440 CPU cores, the total time of CMA-GFS-AERO TLM, ADM, and 4D-Var are approximately 1.1 times, 1.2 times, and 1.4 times those of CMA-GFS TLM, ADM, and 4D-Var, respectively. This highlights the high efficiency and good scalability of CMA-GFS-AERO TLM, ADM, and 4D-Var, making the coupled chemistry meteorology 4D-Var system potentially suitable for operational application.

580

Table 5: Computational costs (unit: s) for 12 h integrations of CMA-GFS TLM/ADM and CMA-GFS-AERO TLM/ADM.

Model\CPU core	480	960	1440
CMA-GFS TLM	14.63	8.95	7.04
CMA-GFS ADM	19.25	11.14	8.07
CMA-GFS-AERO TLM	16.58	10.18	7.55
CMA-GFS-AERO ADM	22.92	12.96	9.31

Note: CMA-GFS TLM/ADM and CMA-GFS-AERO TLM/ADM are integrated with the same time step (900 s) and the same horizontal



resolution of 1°.

585 **Table 6: Computational costs (unit: s) for 6 h integrations of CMA-GFS 4D-Var and CMA-GFS-AERO 4D-Var.**

4D-Var system\CPU core	480	960	1440
CMA-GFS 4D-Var	803	515	428
CMA-GFS-AERO 4D-Var	1013	640	591

Note: CMA-GFS 4D-Var and CMA-GFS-AERO 4D-Var are integrated with the same time step of 300 s/900 s (outer loop/inner loop), the same horizontal resolution of 0.25°/1° (outer loop/inner loop), and the same number of minimization iteration of 35 steps.

**5 Conclusions**

590 In this study, we developed CMA-GFS-AERO 4D-Var, a strongly coupled chemistry meteorology data assimilation system, under the framework of the incremental analysis scheme of CMA-GFS 4D-Var. CMA-GFS-AERO 4D-Var includes three component models: forward, tangent linear, and adjoint models. CMA-GFS-AERO forward model was constructed by integrating the AERO-BC module, an aerosol module containing main aerosol physical processes of BC in the atmosphere, the code of which was extracted from the CUACE air quality model and further optimized in this work, into the CMA-GFS  
595 weather model. The tangent linear and the adjoint of the AERO-BC module was developed and coupled online with the TLM and ADM of CMA-GFS, respectively. Thus, CMA-GFS-AERO ADM includes not only the adjoint of physical processes of BC, but also the adjoint of the meteorological model. The BC mass concentration was used as the control variable and minimized together with atmospheric variables. The background error covariance of the control variable BC adopted a modeled structure. The assimilation system used BC surface observations from the China Atmospheric Monitoring Network.  
600 The observation error and the observation operator of BC were described in detail as well.

CMA-GFS-AERO TLM and ADM were verified by tangent linear approximation and adjoint correctness test. The results show that CMA-GFS-AERO TLM exhibits good performance in tangent linear approximation for BC, and adjoint sensitivity agrees well with tangent linear sensitivity. The CMA-GFS-AERO 4D-Var system was validated for its accuracy and rationality by the single-point observation ideal experiment and the full observation experiment. The results show that  
605 assimilating BC observations can generate analysis increments not only for BC but also for atmospheric variables such as temperature, pressure, wind field, and relative humidity. Furthermore, weakly coupled assimilation may amplify the feedback effects of BC assimilation on atmospheric analysis, while the strongly coupled assimilation, constrained by atmospheric observations, does not amplify the feedback effects, highlighting the capability of the CMA-GFS-AERO 4D-Var strongly coupled assimilation system in exploring the feedback effects of BC assimilation on atmospheric variables.

610 Additionally, the computational performance of CMA-GFS-AERO 4D-Var was evaluated, and the results indicate that when



using 1440 CPU cores for 6 h integrations, the total time of CMA-GFS-AERO 4D-Var are approximately 1.4 times that of CMA-GFS 4D-Var, highlighting the high efficiency of CMA-GFS-AERO 4D-Var and the potential in operational application.

The next steps are as follows. We intend to explore the impact of assimilating surface BC observation on the forecast fields of BC and atmospheric variables through batch test. The CMA-GFS-AERO 4D-Var still needs to be applied to control variables for BC emission scaling factors. Further development of CMA-GFS-AERO 4D-Var will aim to assimilate more aerosol species while ensuring computational efficiency, providing an effective way to study the impact of aerosol assimilation on the analysis and forecast fields of atmospheric variables.

**Data and code availability.** The CMA-GFS model and its 4D-Var system and CUACE model were distributed by CMA Earth System Modeling and Prediction Centre (CEMC) and the Chinese Academy of Meteorological Sciences (<http://www.camscma.cn/>), respectively. The model was run on the PI-SUGON high-performance computer with an Intel Fortran Compiler. Due to copyright restrictions of CEMC, the full codes of the system are not freely available, interested users can contact the operational management department of CEMC or the author, Y. Liu ([liuyzh@cma.gov.cn](mailto:liuyzh@cma.gov.cn)), for further assistance. Codes related to this study, including the tangent linear and adjoint interface codes for black carbon (BC), the observation operator codes for BC and the CMA-GFS-AERO 4D-Var main program, are available on Zenodo (<https://zenodo.org/records/13735640>; Liu et al., 2024). Model outputs of the four assimilation experiments of BC and atmosphere used in this study are also available at this website.

**Author contributions.** XZ, XS and WH envisioned and oversaw the project. YL and CW developed the model code and performed the simulations. YL, WJ, and CW prepared the manuscript with contributions from all co-authors.

**Competing interests.** The contact author has declared that none of the authors has any competing interests.

**Acknowledgements.** This work was supported by Major Program of National Natural Science Foundation of China (42090032). The assimilation and forecast experiments were performed on the high-performance computer Pi-SUGON of China Meteorological Administration. The development of CMA-GFS-AERO 4D-Var system is a systematic project. Apart from the authors, many other colleagues have participated in the project. We sincerely thank the entire team for their cooperation. We also thank YaQiang Wang from CAMS for provide anthropogenic emission sources data and black carbon observations.

## References

- An, X.Q., Zhai, S.X., Jin, M., Gong, S., Wang, Y.: Development of an adjoint model of GRAPES–CUACE and its application in tracking influential haze source areas in north China, *Geosci. Model Dev.*, 9, 2153–2165, <https://doi.org/10.5194/gmd-9-2153-2016>, 2016.
- Baklanov, A., Schlutzen, K.H., Suppan, P., Baldasano, J., Zhang, Y.: Online coupled regional meteorology chemistry models in Europe: current status and prospects, *Atmos. Chem. Phys.*, 14, 317–398,



- <https://doi.org/10.5194/acp-14-317-2014>, 2014.
- Benedetti, A., Morcrette, J.J., Boucher, O., Dethof, A., Engelen, R.J., Fisher, M., Flentje, H., Huneeus, N., Jones, L., Kaiser,  
 645 J.W.: Aerosol analysis and forecast in the European centre for medium-range weather forecasts integrated forecast system:  
 2. Data assimilation, *J. Geophys. Res.-Atmos.*, 114, <https://doi.org/10.1029/2008JD011115>, 2009.
- Bocquet, M., Elbern, H., Eskes, H., Hirtl, M., Žabkar, R., Carmichael, G. R., Flemming, J., Inness, A., Pagowski, M., Pérez  
 Camaño, J. L., Saide, P. E., San Jose, R., Sofiev, M., Vira, J., Baklanov, A., Carnevale, C., Grell, G., and Seigneur, C.:  
 Data assimilation in atmospheric chemistry models: current status and future prospects for coupled chemistry  
 650 meteorology models, *Atmos. Chem. Phys.*, 15, 5325-5358, <https://doi.org/10.5194/acp-15-5325-2015>, 2015.
- Bond, T.C., Doherty, S.J., Fahey, D.W., Forster, P.M., Berntsen, T., DeAngelo, B.J., Flanner, M.G., Ghan, S., Kärcher, B.,  
 Koch, D.: Bounding the role of black carbon in the climate system: A scientific assessment, *J. Geophys. Res.-Atmos.*, 118,  
 5380-5552, <https://doi.org/10.1002/jgrd.50171>, 2013.
- Chen, D., Liu, Z., Ban, J., Zhao, P., Chen, M.: Retrospective analysis of 2015–2017 wintertime PM 2.5 in China: response to  
 655 emission regulations and the role of meteorology, *Atmos. Chem. Phys.*, 19, 7409-7427,  
<https://doi.org/10.5194/acp-19-7409-2019>, 2019.
- Chen, D. and Shen, X.: Recent progress on GRAPES research and application, *J. Appl. Meteor. Sci.*, 17, 773-777, 2006 (in  
 Chinese).
- Chen, D., Xue, J., Yang, X., Zhang, H., Shen, X., Hu, J., Wang, Y., Ji, L., Chen, J.: New generation of multi-scale NWP  
 660 system (GRAPES): general scientific design, *Chinese Sci. Bull.*, 53, 3433-3445,  
<https://doi.org/10.1007/s11434-008-0494-z>, 2008.
- Chen, W., Wang, Y., Li, J., Yi, Z., Zhao, Z., Guo, B., Che, H., Zhang, X.: Description and evaluation of a newly developed  
 emission inventory processing system (EMIPS), *Sci. Total Environ.*, 870, 161909,  
<https://doi.org/10.1016/j.scitotenv.2023.161909>, 2023.
- 665 Chung, S.H. and Seinfeld, J.H.: Global distribution and climate forcing of carbonaceous aerosols, *J. Geophys. Res.-Atmos.*,  
 107, AAC 14-11-AAC 14-33, <https://doi.org/10.1029/2001JD001397>, 2002.
- Courtier, P., Thépaut, J.N., Hollingsworth, A.: A strategy for operational implementation of 4D-Var, using an incremental  
 approach, *Q. J. Roy. Meteor. Soc.*, 120, 1367-1387, <https://doi.org/10.1002/qj.49712051912>, 1994.
- Elbern, H. and Schmidt, H.: A four-dimensional variational chemistry data assimilation scheme for Eulerian chemistry  
 670 transport modeling, *J. Geophys. Res.-Atmos.*, 104, 18583-18598, <https://doi.org/10.1029/1999JD900280>, 1999.
- Elbern, H., Strunk, A., Schmidt, H., Talagrand, O.: Emission rate and chemical state estimation by 4-dimensional variational  
 inversion, *Atmos. Chem. Phys.*, 7, 3749-3769, <https://doi.org/10.5194/acp-7-3749-2007>, 2007.
- Flemming, J., Huijnen, V., Arteta, J., Bechtold, P., Beljaars, A., Blechschmidt, A.M., Diamantakis, M., Engelen, R.J., Gaudel,



- A., Inness, A.: Tropospheric chemistry in the Integrated Forecasting System of ECMWF, *Geosci. Model Dev.*, 8, 975-1003, <https://doi.org/10.5194/gmd-8-975-2015>, 2015.
- Flemming, J., Inness, A., Jones, L., Eskes, H.J., Huijnen, V., Schultz, M.G., Stein, O., Cariolle, D., Kinnison, D., Brasseur, G.: Forecasts and assimilation experiments of the Antarctic ozone hole 2008, *Atmos. Chem. Phys.*, 11, 1961-1977, <https://doi.org/10.5194/acp-11-1961-2011>, 2011.
- Gong, S.L., Barrie, L.A., Blanchet, J.P., Von Salzen, K., Lohmann, U., Lesins, G., Spacek, L., Zhang, L.M., Girard, E., Lin, H.: Canadian Aerosol Module: A size-segregated simulation of atmospheric aerosol processes for climate and air quality models 1. Module development, *J. Geophys. Res.-Atmos.*, 108, AAC 3-1-AAC 3-16, <https://doi.org/10.1029/2001JD002002>, 2003.
- Gong, S.L. and Zhang, X.Y.: CUACE/Dust—an integrated system of observation and modeling systems for operational dust forecasting in Asia, *Atmos. Chem. Phys.*, 8, 2333-2340, <https://doi.org/10.5194/acp-8-2333-2008>, 2008.
- Gong, T., Sun, Z., Zhang, X., Zhang, Y., Wang, S., Han, L., Zhao, D., Ding, D., Zheng, C.: Associations of black carbon and PM<sub>2.5</sub> with daily cardiovascular mortality in Beijing, China, *Atmos. Environ.*, 214, 116876, <https://doi.org/10.1016/j.atmosenv.2019.116876>, 2019.
- Granier, C., Darras, S., Gon, H.D.v.d., Jana, D., Elguindi, N., Bo, G., Michael, G., Marc, G., Jalkanen, J.-P., Kuenen, J., Liousse, C., Quack, B., Simpson, D., Sindelarova, K.: The Copernicus Atmosphere Monitoring Service Global and Regional Emissions (April 2019 Version), Copernicus Atmosphere Monitoring Service, 2019.
- Guerrette, J.J. and Henze, D.K.: Development and application of the WRFPLUS-Chem online chemistry adjoint and WRFDA-Chem assimilation system, *Geosci. Model Dev.*, 8, 1857–1876, <https://doi.org/10.5194/gmd-8-1857-2015>, 2015.
- Guo, B., Wang, Y., Zhang, X., Che, H., Ming, J., Yi, Z.: Long-Term variation of black carbon aerosol in China based on revised aethalometer monitoring data, *Atmosphere*, 11, 684, <https://doi.org/10.3390/atmos11070684>, 2020.
- Hakami, A., Henze, D.K., Seinfeld, J.H., Singh, K., Sandu, A., Kim, S., Byun, Li, Q.: The adjoint of CMAQ, *Environ. Sci. Technol.*, 41, 7807-7817, <https://doi.org/10.1021/es070944p>, 2007.
- Henze, D.K., Hakami, A., Seinfeld, J.H.: Development of the adjoint of GEOS-Chem, *Atmos. Chem. Phys.*, 7, 2413-2433, <https://doi.org/10.5194/acp-7-2413-2007>, 2007.
- Henze, D.K., Seinfeld, J.H., Shindell, D.T.: Inverse modeling and mapping US air quality influences of inorganic PM<sub>2.5</sub> precursor emissions using the adjoint of GEOS-Chem, *Atmos. Chem. Phys.*, 9, 5877-5903, <https://doi.org/10.5194/acp-9-5877-2009>, 2009.
- Huo, Z., Li, X., Chen, J., Liu, Y.: CMA global ensemble prediction using singular vectors from background field, *J. Appl. Meteor. Sci.*, 33, 655-667, 2022 (in Chinese).





- 705 Inness, A., Baier, F., Benedetti, A., Bouarar, I., Chabrillat, S., Clark, H., Clerbaux, C., Coheur, P., Engelen, R.J., Errera, Q.,  
 Flemming, J., George, M., Granier, C., Hadji-Lazaro, J., Huijnen, V., Hurtmans, D., Jones, L., Kaiser, J.W.,  
 Kapsomenakis, J., Lefever, K., Leitão, J., Razinger, M., Richter, A., Schultz, M.G., Simmons, A.J., Suttie, M., Stein, O.,  
 Thépaut, J.N., Thouret, V., Vrekoussis, M., Zerefos, C., the, M.t.: The MACC reanalysis: an 8 yr data set of atmospheric  
 composition, *Atmos. Chem. Phys.*, 13, 4073-4109, <https://doi.org/10.5194/acp-13-4073-2013>, 2013.
- 710 Jacobson, M.Z., Turco, R.P., Jensen, E.J., Toon, O.B.: Modeling coagulation among particles of different composition and  
 size, *Atmos. Environ.*, 28, 1327-1338, [https://doi.org/10.1016/1352-2310\(94\)90280-1](https://doi.org/10.1016/1352-2310(94)90280-1), 1994.
- Janssens-Maenhout, G., Crippa, M., Guizzardi, D., Dentener, F., Muntean, M., Pouliot, G., Keating, T., Zhang, Q., Kurokawa,  
 J., Wankmüller, R.: HTAP\_v2. 2: a mosaic of regional and global emission grid maps for 2008 and 2010 to study  
 hemispheric transport of air pollution, *Atmos. Chem. Phys.*, 15, 11411-11432, <https://doi.org/10.5194/acp-15-11411-2015>,  
 715 2015.
- Koch, D.: Transport and direct radiative forcing of carbonaceous and sulfate aerosols in the GISS GCM, *J. Geophys.*  
*Res.-Atmos.*, 106, 20311-20332, <https://doi.org/10.1029/2001JD900038>, 2001.
- Kuhlbusch, T.A.J.: Black carbon and the carbon cycle. *Science*, 280, 1903-1904, doi: 10.1126/science.280.5371.1903, 1998.
- Lanczos, C.: An iteration method for the solution of the eigenvalue problem of linear differential and integral operators,  
 720 *Journal of Research of the National Bureau of Standards*, 45, 255-282, 1950.
- Li, M., Zhang, Q., Kurokawa, J.-i., Woo, J.-H., He, K., Lu, Z., Ohara, T., Song, Y., Streets, D.G., Carmichael, G.R.: MIX: a  
 mosaic Asian anthropogenic emission inventory under the international collaboration framework of the MICS-Asia and  
 HTAP, *Atmos. Chem. Phys.*, 17, 935-963, <https://doi.org/10.5194/acp-17-935-2017>, 2017.
- Liu, F.: Adjoint model of Comprehensive Air quality Model CAMx—construction and application, Post-doctoral research  
 725 report, Peking University, Beijing, 2005 (in Chinese).
- Liu, Y., Gong, J., Zhang, L., Chen, Q.: Influence of linearized physical processes on the GRAPES 4DVAR, *Acta Meteorol.*  
*Sin.*, 77, 196-209, 2019.
- Liu, Y., Zhang, L., Chen, J., Wang, C.: An improvement of the linearized planetary boundary layer parameterization scheme  
 for CMA-GFS 4DVar. *J. Appl. Meteor. Sci.*, 34, 15-26, doi: 10.11898/1001-7313.20230102, 2023.
- 730 Liu, Y., Zhang, L., Jin, Z.: The Optimization of GRAPES Global Tangent Linear Model and Adjoint Model. *Journal of*  
*Applied Meteorological Science*, 28, 62-71, doi: 10.11898/1001-7313.20170106, 2017 (in Chinese).
- Liu, Y., Zhang, L., Lian, Z.: Conjugate Gradient Algorithm in the Four-Dimensional Variational Data Assimilation System in  
 GRAPES, *J. Meteorol. Res.*, 32, 974-984, <https://doi.org/10.1007/s13351-018-8053-2>, 2018.
- Lorenc, A.C., Ballard, S.P., Bell, R.S., Ingleby, N.B., Andrews, P.L.F., Barker, D.M., Bray, J.R., Clayton, A.M., Dalby, T., Li,  
 735 D.: The Met. Office global three-dimensional variational data assimilation scheme, *Q. J. Roy. Meteor. Soc.*, 126,





- 2991-3012, doi:10.1256/smsqj.57001, 2000.
- Lorenc, A.C. and Rawlins, F.: Why does 4D-Var beat 3D-Var? Q. J. Roy. Meteor. Soc., 131, <https://doi.org/10.1256/qj.05.85>, 2010.
- Mahfouf, J.-F.: Influence of physical processes on the tangent-linear approximation, Tellus A: Dynamic Meteorology and Oceanography, 51, 147-166, <https://doi.org/10.3402/tellusa.v51i2.12312>, 1999.
- 740 Mahfouf, J.F. and Rabier, F.: The ECMWF operational implementation of four-dimensional variational assimilation-Part I : Experimental results with simplified physics, Q. J. Roy. Meteor. Soc., 126, 1143-1170, <https://doi.org/10.1002/qj.49712656415>, 2000.
- Menon, S., Hansen, J., Nazarenko, L., Luo, Y.: Climate effects of black carbon aerosols in China and India, Science, 297, 2250-2253, doi: 10.1126/science.1075159, 2002.
- 745 Menut, L., Vautard, R., Beekmann, M., Honoré, C.: Sensitivity of photochemical pollution using the adjoint of a simplified chemistry-transport model, J. Geophys. Res.-Atmos., 105, 15379-15402, <https://doi.org/10.1029/1999JD900953>, 2000.
- Müller, J.F. and Stavrakou, T.: Inversion of CO and NO<sub>x</sub> emissions using the adjoint of the IMAGES model, Atmos. Chem. Phys., 5, 1157-1186, <https://doi.org/10.5194/acp-5-1157-2005>, 2005.
- 750 Pagowski, M., Grell, G.A., McKeen, S.A., Peckham, S.E., Devenyi, D.: Three-dimensional variational data assimilation of ozone and fine particulate matter observations: some results using the Weather Research and Forecasting—Chemistry model and Grid-point Statistical Interpolation, Q. J. Roy. Meteor. Soc., 136, 2013-2024, <https://doi.org/10.1002/qj.700>, 2010.
- Sandu, A., Daescu, D.N., Carmichael, G.R., Chai, T.: Adjoint sensitivity analysis of regional air quality models, J. Comput. Phys., 204, 222-252, <https://doi.org/10.1016/j.jcp.2004.10.011>, 2005.
- 755 Schmidt, H. and Martin, D.: Adjoint sensitivity of episodic ozone in the Paris area to emissions on the continental scale, J. Geophys. Res.-Atmos., 108, <https://doi.org/10.1029/2001JD001583>, 2003.
- Schwartz, C.S., Liu, Z., Lin, H.C., McKeen, S.A.: Simultaneous three-dimensional variational assimilation of surface fine particulate matter and MODIS aerosol optical depth, J. Geophys. Res.-Atmos., 117, <https://doi.org/10.1029/2011JD017383>, 2012.
- 760 Seinfeld, J.H. and Pandis, S.N.: Atmospheric Chemistry and Physics: From Air Pollution to Climate Change, Environment & Policy for Sustainable Development, 1998.
- Semane, N., Peuch, V.H., Pradier, S., Desroziers, G., El Amraoui, L., Brousseau, P., Massart, S., Chapnik, B., Peuch, A.: On the extraction of wind information from the assimilation of ozone profiles in Météo-France 4-D-Var operational NWP suite, Atmos. Chem. Phys., 9, 4855-4867, <https://doi.org/10.5194/acp-9-4855-2009>, 2009.
- 765 Shen, X., Su, Y., Zhang, H., Hu, J.: New Version of the CMA-GFS Dynamical Core Based on the Predictor–Corrector Time



- Integration Scheme, *J. Meteorol. Res.*, 37, 273-285, <https://doi.org/10.1007/s13351-023-3002-0>, 2023.
- Su, Y., Shen, X., Peng, X., Li, X., Wu, X., Zhang, S., Chen, X.: Application of PRM scalar advection scheme in GRAPES  
 global forecast system, *Chinese Journal of Atmospheric Sciences*, 37, 1309-1325,  
 770 [doi:10.3878/j.issn.1006-9895.2013.12164](https://doi.org/10.3878/j.issn.1006-9895.2013.12164), 2013 (in Chinese).
- Tian, X. and Zou, X.: Development of the tangent linear and adjoint models of the MPAS-Atmosphere dynamic core and  
 applications in adjoint relative sensitivity studies, *Tellus A:Dynamic Meteorology and Oceanography*, 72, 16,  
<https://doi.org/10.1080/16000870.2020.1814602>, 2020.
- Vautard, R., Beekmann, M., Menut, L.: Applications of adjoint modelling in atmospheric chemistry: sensitivity and inverse  
 775 modelling, *Environ. Modell. Softw.*, 15, 703-709, [https://doi.org/10.1016/S1364-8152\(00\)00058-X](https://doi.org/10.1016/S1364-8152(00)00058-X), 2000.
- Wang, C., An, X., Zhao, D., Sun, Z., Jiang, L., Li, J., Hou, Q.: Development of GRAPES-CUACE adjoint model version 2.0  
 and its application in sensitivity analysis of ozone pollution in north China, *Sci. Total Environ.*, 826, 153879,  
<https://doi.org/10.1016/j.scitotenv.2022.153879>, 2022.
- Wang, H., Gong, S., Zhang, H., Chen, Y., Shen, X., Chen, D., Xue, J., Shen, Y., Wu, X., Jin, Z.: A new-generation sand and  
 780 dust storm forecasting system GRAPES\_CUACE/Dust: Model development, verification and numerical simulation, *Chin.*  
*Sci. Bull.*, 55, 635-649, <https://doi.org/10.1007/s11434-009-0481-z>, 2010.
- Wang, H., Peng, Y., Zhang, X., Liu, H., Zhang, M., Che, H., Cheng, Y., Zheng, Y.: Contributions to the explosive growth of  
 PM 2.5 mass due to aerosol–radiation feedback and decrease in turbulent diffusion during a red alert heavy haze in  
 Beijing–Tianjin–Hebei, China, *Atmos. Chem. Phys.*, 18, 17717-17733, <https://doi.org/10.5194/acp-18-17717-2018>, 2018.
- 785 Xu, X., Yang, X., Zhu, B., Tang, Z., Wu, H., Xie, L.: Characteristics of MERRA-2 black carbon variation in east China  
 during 2000–2016, *Atmos. Environ.*, 222, 117140, <https://doi.org/10.1016/j.atmosenv.2019.117140>, 2020.
- Yang, X., Chen, J., Hu, J., Chen, D., Shen, X., Zhang, H.: A semi-implicit semi-Lagrangian global nonhydrostatic model and  
 the polar discretization scheme, *Sci. China Ser. D*, 50, 1885-1891, <https://doi.org/10.1007/s11430-007-0124-7>, 2007.
- Zhang, L., Liu, Y., Liu, Y., Gong, J., Lu, H., Jin, Z., Tian, W., Liu, G., Zhou, B., Zhao, B.: The operational global  
 790 four-dimensional variational data assimilation system at the China Meteorological Administration, *Q. J. Roy. Meteor.*  
*Soc.*, 145, 1882-1896, <https://doi.org/10.1002/qj.3533>, 2019.
- Zhang, Y.: Online-coupled meteorology and chemistry models: history, current status, and outlook, *Atmos. Chem. Phys.*, 8,  
<https://doi.org/10.5194/acp-8-2895-2008>, 2008.
- Zheng, B., Tong, D., Li, M., Liu, F., Hong, C., Geng, G., Li, H., Li, X., Peng, L., Qi, J.: Trends in China's anthropogenic  
 795 emissions since 2010 as the consequence of clean air actions, *Atmos. Chem. Phys.*, 18, 14095-14111,  
<https://doi.org/10.5194/acp-18-14095-2018>, 2018.
- Zhou, C., Gong, S., Zhang, X., Liu, H., Xue, M., Cao, G., An, X., Che, H., Zhang, Y., Niu, T.: Towards the improvements of



simulating the chemical and optical properties of Chinese aerosols using an online coupled model–CUACE/Aero, Tellus

B: Chemical and Physical Meteorology, 64, 18965, <https://doi.org/10.3402/tellusb.v64i0.18965>, 2012.